Progress In Electromagnetics Research M, Vol. 54, 19–27, 2017

Real-Coefficient FGG-FG-FFT for the Combined Field Integral Equation

Hua-Long Sun*, Chuang Ming Tong, Peng Peng, Gao Xiang Zou, and Gui Long Tian

Abstract—This article proposes a new scheme of real-coefficient fitting both Green's function and its gradient with Fast Fourier Transform (RFGG-FG-FFT) for combined field integral equation (CFIE) to compute the conducting object's electromagnetic scattering, which improves original fitting both Green's function and its gradient with Fast Fourier Transform (FGG-FG-FFT) on efficiency. Firstly, based on Moore-Penrose generalized inverse, an equivalent form of fitting matrix equation is obtained containing the property of Green's function's integral proved by addition theorem. Based on this property, with truncated Green's function new fitting technique is presented for computing fitting coefficients with real value expression, which is different from complex value expression by the original fitting technique in FGG-FG-FFT. Numerical analysis of error shows that new fitting technique has the same accuracy, but only one half of sparse matrices' storage compared to the original fitting technique in FGG-FG-FFT. Finally, the new scheme combining FGG-FG-FFT and new fitting technique is constructed. Some examples show that the new scheme is accurate and effective compared to FGG-FG-FFT and p-FFT.

1. INTRODUCTION

Many researchers have studied efficient solvers for the integral equation (IE) in analysing electromagnetic radiation or scattering problems. Among them, the method of moments (MOM) [1] is one of typical numerical algorithms by discretizing the IE with basis functions into resultant matrix equation. FFT-based algorithms employ FFT to speed up the matrix-vector products, needing to discretize IE on a uniform Cartesian grid. The Adaptive Integral Method (AIM) [2] and precorrected-FFT (p-FFT) [3] focus on the projections of the basis functions on the nodes of the uniform Cartesian. In the case of the same grid spacing and expansion order, compared with AIM, p-FFT possesses higher accuracy because the Green's function is considered in the matching stage [4]. Different from the above two FFT-based algorithms, integral equation Fast Fourier Transform (IE-FFT) [5] was proposed to represent the Green's function with its values on the nodes of the uniform Cartesian grid by interpolation. Subsequently, Xie et al. [6] improved accuracy of IE-FFT by fitting both Green's function and its gradient onto Cartesian grid node, named as FGG-FG-FFT. However, in the case of the same grid spacing and expansion order, FGG-FG-FFT presents less efficiency than IE-FFT because of computing method of fitting coefficients and the complex value expression of fitting coefficients. Among these two reasons, the latter is the major one, which not only has twice storage requirement, but also increases the complexity per iteration compared to real value expression of fitting coefficients. Ref. [7] shows the useful fact that imaginary part of fitting coefficients is obviously smaller than real part. However, mathematical deduction is not provided.

In this paper, firstly based on Moore-Penrose generalized inverse, an equivalent form of fitting matrix equation is obtained containing the property of Green's function's integral proved by addition theorem [8]. Secondly, based on this property, with truncated Green's function new fitting technique

Received 22 November 2016, Accepted 13 January 2017, Scheduled 2 February 2017
* Corresponding author: Hua-Long Sun (hualongsun1982@163.com).
The authors are with the Air and Missile Defense College, Air Force Engineering University, Xi'an 710051, China.

is presented for computing fitting coefficients. Fitting coefficients with new fitting technique are purely real. Numerical analysis of error shows that compared to the original fitting technique in FGG-FG-FFT, the new fitting technique has a similar accuracy, but only one half of sparse matrices' storage. Finally, a new scheme combining FGG-FG-FFT and new fitting technique for CFIE is constructed to compute electromagnetic scattering. Some examples show that the new scheme with real value expression of fitting coefficients possesses not only the same high accuracy as FGG-FG-FFT and p-FFT, but also higher efficiency than FGG-FG-FFT and p-FFT due to their complex value expression of fitting coefficients and projection coefficients, respectively.

2. FORMULATION

2.1. New Fitting Technique in RFGG-FG-FFT

The current distribution on the 3D arbitrarily shaped conductor can be obtained by finding the solution of electric field integral equation (EFIE), and magnetic field integral equation (MFIE) [1]:

$$\begin{aligned} 4\pi\mathbf{E}^{inc}|_t &= \left[jk_0\eta_0\int_S \left[g\left(\mathbf{r},\mathbf{r}'\right)\mathbf{J}(\mathbf{r}') + \left(1/k_0^2\right)\nabla g\left(\mathbf{r},\mathbf{r}'\right)\nabla'\cdot\mathbf{J}(\mathbf{r}')\right]dS'\right]\Big|_t, \\ 4\pi\mathbf{H}^{inc}|_t &= \left[2\pi\left(\hat{n}\times\mathbf{J}(\mathbf{r})\right) + \text{P.V.}\int_S \mathbf{J}(\mathbf{r}')\times\nabla g\left(\mathbf{r},\mathbf{r}'\right)dS'\right]\Big|_t, \end{aligned} \tag{1}$$

where $\mathbf{E}^{inc}$ and $\mathbf{H}^{inc}$ are the incident electric and magnetic field, respectively; $\mathbf{J}(\mathbf{r})$ is the surface equivalent current; η_0 and k_0 are the wave impedance and the wave number in the free space; P.V. is the principal value integral; $g(\mathbf{r},\mathbf{r}')$ is the Green's function in the free space with the form of $g(\mathbf{r},\mathbf{r}') = e^{(-jk_0|\mathbf{r}-\mathbf{r}'|)}/|\mathbf{r}-\mathbf{r}'|$; subscript t denotes the tangent part; $\hat{n}$ is the unit outer normal vector on the object's surface. Then choose Rao-Wilton-Glisson (RWG) [9] functions as the basis functions and testing functions to formulate resultant matrix equation:

$$Z^{\text{CFIE}}I = V \tag{2}$$

with $Z^{\text{CFIE}} = aZ^{\text{EFIE}} + (1-a)Z^{\text{MFIE}}$, whose impedance elements have the form of:

$$\begin{aligned} Z_{mn}^{\text{EFIE}} &= jk_0\eta_0\int_{T_m} dS\mathbf{f}_m(\mathbf{r})\cdot\int_{T_n} g(\mathbf{r},\mathbf{r}')\mathbf{f}_n(\mathbf{r}')dS' - \frac{j\eta_0}{k_0}\int_{T_m} dS\nabla\cdot\mathbf{f}_m(\mathbf{r})\int_{T_n} g(\mathbf{r},\mathbf{r}')\nabla'\cdot\mathbf{f}_n(\mathbf{r}')dS', \\ Z_{mn}^{\text{MFIE}} &= 2\pi\int_{T_m}\mathbf{f}_m(\mathbf{r})\cdot\mathbf{f}_n(\mathbf{r})dS' + \int_{T_m} dS[\widehat{n}\times\mathbf{f}_m(\mathbf{r})]\cdot\int_{T_n}\nabla g(\mathbf{r},\mathbf{r}')\times\mathbf{f}_n(\mathbf{r}')dS', \end{aligned} \tag{3}$$

in which T_m and T_n are the triangular patches of $\mathbf{f}_m(\mathbf{r})$ and $\mathbf{f}_n(\mathbf{r})$, respectively. According to the interaction between basis functions, resultant impedance matrix can be split into two parts, in which some are near-field interaction parts, and the others are far-field interaction parts [6]:

$$\begin{aligned} Z^{\text{CFIE}} \approx\ & \left[a\left(Z_{\text{MOM}}^{\text{EFIE-near}} - Z_{\text{FFT}}^{\text{EFIE-near}}\right) + (1-a)\left(Z_{\text{MOM}}^{\text{MFIE-near}} - Z_{\text{FFT}}^{\text{MFIE-near}}\right)\right] \\ & + aZ_{\text{FFT}}^{\text{EFIE-total}} + (1-a)Z_{\text{FFT}}^{\text{MFIE-total}}. \end{aligned} \tag{4}$$

As we know, if the distance between basis functions is less than near zone boundary d_{near}, near-field interaction impedances computed by FFT-based algorithms present poor accuracy, so all of FFT-based algorithms need the pre-correction of near-field interaction impedances. In Eq. (4), $Z_{\text{MOM}}^{\text{CFIE-near}} - Z_{\text{FFT}}^{\text{CFIE-near}}$is precorrected matrix, in which $Z_{\text{MOM}}^{\text{CFIE-near}}$ and $Z_{\text{FFT}}^{\text{CFIE-near}}$ are near-field interaction impedances computed by MOM and FFT-based algorithm respectively. $Z_{\text{FFT}}^{\text{EFIE}}$ and $Z_{\text{FFT}}^{\text{MFIE}}$ are the approximation by FFT-based algorithms expressed as:

$$Z_{\text{FFT}}^{\text{EFIE}} = jk_0\eta_0\mathbf{\Pi}\cdot G\mathbf{\Pi}^T - j(\eta_0/k_0)\Pi_d G\Pi_d^T, \quad Z_{\text{FFT}}^{\text{MFIE}} = \mathbf{\Pi}_g\cdot G\mathbf{\Pi}^T, \tag{5}$$

where Π, Π_d and Π_g are sparse matrices composed of basis functions and fitting coefficients. G stands for a triple Toeplitz on Cartesian grid. Superscript T identifies transpose operator. With this form, matrix-vector products per iteration can be accelerated by FFT. Each iteration is only 8 FFTs, and the whole computation complexity is reduced from $O(N^2)$ to $O(N^{1.5}\log N)$ [6].

Similar to other FFT-based methods, FGG-FG-FFT also needs fitting cube C_m composed of $N_C = (M+1)^3$ grid nodes with the center being c_m in which M is expansion order. Grid spacing is h in three coordinate directions. Suppose r_m to be the minimum radius of spherical surface enclosing C_m. R_m is the radius of testing spherical surface S_m with the same center c_m. Assuming $R_m = r_m + 0.05\lambda$, λ is the wavelength in free space. $\{r_t\}_1^{T_e}$ are testing points locating on S_m, which are chosen according to Ref. [10]. So Green's function and its gradient can be expressed as:

$$g\left(\mathbf{r},\mathbf{r}'\right) = \sum_{u\in Cm} \pi_{u,Cm}^{\mathbf{r}} g\left(\mathbf{r}_u,\mathbf{r}'\right), \quad \nabla g\left(\mathbf{r},\mathbf{r}'\right) = \sum_{u\in Cm} \varsigma_{u,Cm}^{\mathbf{r}} g\left(\mathbf{r}_u,\mathbf{r}'\right) \tag{6}$$

where $\{\pi_{u,Cm}^{r}\}_{u=1}^{Nc}$ and $\{\varsigma_{u,Cm}^{r}\}_{u=1}^{Nc}$ are fitting coefficients. Fitting the gradient of Green's function adopts the one-step fitting scheme (OSFS) which is the optimal scheme for fitting the gradient on efficiency and accuracy shown in [6]. In this paper, both of FGG-FG-FFT and RFGG-FG-FFT employ OSFS for fitting the gradient. $\mathbf{r}$ and $\mathbf{r}'$ are the position vector of field and source points, respectively. $\mathbf{r}$ is surrounded by C_m, and $\mathbf{r}_u$ is the grid node's vector. For solving fitting coefficients, assume $\mathbf{r}' = \mathbf{r}_t$, overdeterminant fitting matrix equation with the dimension of $T_e \times N_C$ is given:

$$\begin{aligned} &[X]\{\pi_{Cm}^{\mathbf{r}}\} = \left[Y^1\right], \quad \{\pi_{Cm}^{\mathbf{r}}\} = [X]^+\left[Y^1\right], \quad [X]\{\varsigma_{Cm}^{\mathbf{r}}\} = \left[Y^2\right], \quad \{\varsigma_{Cm}^{\mathbf{r}}\} = [X]^+\left[Y^2\right], \\ &X_{i,j} = g(\mathbf{r}_j,\mathbf{r}_{ti}), \quad i\in[1,T_e], \quad j\in[1,N_C], \\ &Y_i^1 = g(\mathbf{r},\mathbf{r}_{ti}), \quad Y_i^2 = \nabla g(\mathbf{r},\mathbf{r}_{ti}), \quad i\in[1,T_e], \end{aligned} \tag{7}$$

in which, $[X]^+$ denotes the generalized inverse of $[X]$; fitting coefficients $\{\pi_{u,Cm}^{r}\}_{u=1}^{Nc}$ and $\{\varsigma_{u,Cm}^{r}\}_{u=1}^{Nc}$ are determined by solving this fitting matrix equation, so sparse matrices $\mathbf{\Pi}$, Π_d and $\mathbf{\Pi}_g$ can be decided, the detailed description about FGG-FG-FFT can be found in [6].

During per iteration, the most time-consuming is matrix-vector multiplications concerning sparse matrices composed of fitting coefficients and basis functions. Noticeably, fitting coefficients by AIM and IE-FFT are real values, and those by FGG-FG-FFT and p-FFT are complex values, so AIM and IE-FFT have higher efficiency, lower accuracy than p-FFT and FGG-FG-FFT under the same grid spacing and expansion order. In essence, fitting technique in p-FFT and FGG-FG-FFT is near-matching [4]. Hence, a naive thought would be to ask if real values scheme and fitting technique can be combined to obtain higher efficiency and accuracy. The answer is yes. Actually, mass of examples for Equation (7) shows that: with T_e getting more, imaginary part of fitting coefficient is not more than 1% of real part of its own, which indicates feasibility of real fitting coefficient scheme. In practice, when testing points' number on testing spherical surface approximates infinite and generalized inverse satisfies Moore-Penrose conditions, fitting coefficients of FGG-FG-FFT and p-FFT approximate real values. For Equation (7), adopting Moore-Penrose generalized inverse to compute $[X]^+$, the solution of $[X]^+$ is existent and exclusive and simultaneously has the equivalent form of $[X]^+ = [X^H X]^+ [X^H]$ in which superscript H denotes Hermitian. Referring to [10], $\{r_t\}_1^{T_e}$ are not mean distribution on testing spherical surface. In practice, when $\{r_t\}_1^{T_e}$ are mean distribution on testing spherical surface, with the number of $\{r_t\}_1^{T_e}$ getting more and more, fitting accuracy is comparable to the method by [10]. When utilizing mean distribution, testing points $\{r_t\}_1^{T_e}$ have the equal weight $w_t = 4\pi R_m^2/T_e$, which is the area of small cell on testing spherical surface. Obviously, $[X]^+$ can be expressed as $[X]^+ = [w_t X^H X]^+ [w_t X^H]$. Furthermore, taking the limit as the number of testing points $T_e \to \infty$, we have:

$$\begin{aligned} &\{\pi_{Cm}^{\mathbf{r}}\} = [A]^+\left[B^1\right], \quad \{\varsigma_{Cm}^{\mathbf{r}}\} = [A]^+\left[B^2\right], \\ &A_{i,j} = \int_{S_m} g^*(\mathbf{r}_i,\mathbf{r}_t) g(\mathbf{r}_j,\mathbf{r}_t) dS, \quad i,j\in[1,N_C], \\ &B_i^1 = \int_{S_m} g^*(\mathbf{r}_i,\mathbf{r}_t) g(\mathbf{r},\mathbf{r}_t) dS, \quad i\in[1,N_C], \quad B_i^2 = \int_{S_m} g^*(\mathbf{r}_i,\mathbf{r}_t) \nabla g(\mathbf{r},\mathbf{r}_t) dS, \quad i\in[1,N_C]. \end{aligned} \tag{8}$$

The resultant fitting coefficients almost equals those by Eq. (7). Then, we will give an important property of $A_{i,j}$ and B_i^p in the next section.

2.2. The Property of Green's Function's Integral

Use the addition theorem:

$$\begin{aligned} g(\mathbf{r},\mathbf{r}_t) &\approx (-jk_0/4\pi)\sum\nolimits_{p=1}^{K}\omega_p e^{j\mathbf{k}_p\cdot\mathbf{r}}T\left(\mathbf{r}_t,\hat{k}_p\right), \\ T(\mathbf{r}_t,\hat{k}) &= \sum\nolimits_{l_1=0}^{L}(-j)^{l_1}(2l_1+1)h_{l_1}^{(2)}(k_0r_t)P_{l_1}\left(\hat{k}\cdot\hat{r}_t\right). \end{aligned} \tag{9}$$

where T is translation matrix and L the number of modes. According to Gaussian quadrature formula, $\{\hat{k}_p\}_1^K$ are angular directions on Ewald sphere with the total number $K=2L^2$ satisfying the symmetry to the center of Ewald sphere [11], and ω_p is the Gauss weight.

Substitute Eq. (9) into Eq. (8) and define $\overline{A}_{i,j}$, $\overline{B}_{i,j}$ as

$$\begin{aligned} \overline{A}_{i,j} &= (k_0/4\pi)^2\sum\nolimits_{p=1}^{K_1}\sum\nolimits_{q=1}^{K_2}e^{-j\mathbf{k}_p\cdot\mathbf{r}_i}e^{j\mathbf{k}_q\cdot\mathbf{r}_j}\int_s T_1^*\left(\mathbf{r}_t,\hat{k}_p\right)T_2\left(\mathbf{r}_t,\hat{k}_q\right)ds, \\ \overline{B}_{i,j} &= (k_0/4\pi)^2\sum\nolimits_{p=1}^{K_1}\sum\nolimits_{q=1}^{K_2}(-j\mathbf{k}_p)e^{-j\mathbf{k}_p\cdot\mathbf{r}_i}e^{j\mathbf{k}_q\cdot\mathbf{r}_j}\int_s T_1^*\left(\mathbf{r}_t,\hat{k}_p\right)T_2\left(\mathbf{r}_t,\hat{k}_q\right)ds, \end{aligned} \tag{10}$$

in which, K_1 and K_2 are relative to $g(\mathbf{r}_i,\ \mathbf{r}_t)$ and $g(\mathbf{r}_j,\ \mathbf{r}_t)$, respectively. Generally, $K_1 \neq K_2$. The integral term concerning T_1 and T_2 in (10) can be expressed as follows:

$$\begin{aligned} \int_S T_1^*\left(\mathbf{r}_t,\hat{k}_p\right)T_2\left(\mathbf{r}_t,\hat{k}_q\right)ds \ =\ & \int_S\sum\nolimits_{l_1=0}^{L_1}j^{l_1}(2l_1+1)h_{l_1}^{*(2)}(k_0r_t)P_{l_1}\left(\hat{k}_p\cdot\hat{r}_t\right) \\ & \cdot\sum\nolimits_{l_2=0}^{L_2}(-j)^{l_2}(2l_2+1)h_{l_2}^{(2)}(k_0r_t)P_{l_2}\left(\hat{k}_q\cdot\hat{r}_t\right)dS, \end{aligned} \tag{11}$$

with

$$P_l\left(\hat{k}_s\cdot\hat{r}\right)=\sum\nolimits_{m=0}^{l}\varepsilon_m\frac{(l-m)!}{(l+m)!}P_l^m(\cos\theta_s)P_l^m(\cos\theta)\cos(m(\phi_s-\phi)).$$

where $h_l^{(2)}$ is 2nd kind spherical Hankel function of order l, P_l the Legendre function of order l, P_l^m the 1st kind associated Legendre function of order m by l, and ε_m the Neumann's number (1 for $m=0$ and 2 for $m>0$). Then according to [12], tesseral harmonics has the form of:

$$T_{m,n}^e(\theta,\phi)=P_n^m(\cos\theta)\cos(m\phi),\ T_{m,n}^o(\theta,\phi)=P_n^m(\cos\theta)\sin(m\phi). \tag{12}$$

By its orthogonality on the whole of spherical surface [12], Equation (11) can be translated into:

$$\begin{aligned} &\int_s T_1^*\left(\mathbf{r}_t,\hat{k}_p\right)T_2\left(\mathbf{r}_t,\hat{k}_q\right)ds \\ =&r_t^2\sum\nolimits_{l_1=0}^{L}(2l_1+1)^2\left|h_{l_1}^{(2)}(k_0r_t)\right|^2\left\{P_{l_1}(\cos\theta_p)P_{l_1}(\cos\theta_q)\frac{4\pi}{(2l_1+1)}\right. \\ &\left.+\sum\nolimits_{m=1}^{l_1}\varepsilon_m^2\left[\frac{(l-m)!}{(l+m)!}\right]^2P_{l_1}^m(\cos\theta_p)P_{l_1}^m(\cos\theta_q)\frac{4\pi}{(2l_1+1)}\frac{(l+m)!}{(l-m)!}\left[\frac{\cos(m(\phi_p-\phi_q))}{\varepsilon_m}\right]\right\} \\ =&4\pi r_t^2\sum_{l_1=0}^{L}(2l_1+1)\left|h_{l_1}^{(2)}(k_0r_t)\right|^2\sum_{m=0}^{l_1}\varepsilon_m\left[\frac{(l-m)!}{(l+m)!}\right]P_{l_1}^m(\cos\theta_p)P_{l_1}^m(\cos\theta_q)\cos(m(\phi_p-\phi_q)), \end{aligned} \tag{13}$$

where $L=\min\{L_1,\ L_2\}$. Use the expansion of P_l in Equation (11) again:

$$\int_s T_1^*\left(\mathbf{r}_t,\hat{k}_p\right)T_2\left(\mathbf{r}_t,\hat{k}_q\right)ds=4\pi r_t^2\sum\nolimits_{l_1=0}^{L}(2l_1+1)\left|h_{l_1}^{(2)}(k_0r_t)\right|^2P_{l_1}\left(\hat{k}_p\cdot\hat{k}_q\right). \tag{14}$$

Obviously, this is pure real. Then, substitute Eq. (14) into Eq. (10):

$$\begin{aligned} \overline{A}_{i,j} =& \left[(k_0r_t)^2/4\pi\right]\sum\nolimits_{p=1}^{K_1/2}\sum\nolimits_{q=1}^{K_2}\omega_p\omega_q\left(e^{j\mathbf{k}_p\cdot\mathbf{r}_i}e^{-j\mathbf{k}_q\cdot\mathbf{r}_j}+e^{-j\mathbf{k}_p\cdot\mathbf{r}_i}e^{j\mathbf{k}_q\cdot\mathbf{r}_j}\right) \\ & \sum\nolimits_{l_1=0}^{L}(2l_1+1)\left|h_{l_1}^{(2)}(k_0r_t)\right|^2P_{l_1}\left(\hat{k}_p\cdot\hat{k}_q\right) \\ =& \left[(k_0r_t)^2/2\pi\right]\sum\nolimits_{p=1}^{K_1/2}\sum\nolimits_{q=1}^{K_2}\omega_p\omega_q\cos(\mathbf{k}_p\cdot\mathbf{r}_i-\mathbf{k}_q\cdot\mathbf{r}_j)\sum\nolimits_{l_1=0}^{L}(2l_1+1)\left|h_{l_1}^{(2)}(k_0r_t)\right|^2P_{l_1}\left(\hat{k}_p\cdot\hat{k}_q\right), \end{aligned} \tag{15}$$

$$\bar{B}_{i,j} = [(k_0 r_t)^2/2\pi] \sum_{p=1}^{K_1/2} \sum_{q=1}^{K_2} \omega_p \omega_q \sin(\mathbf{k}_p \cdot \mathbf{r}_i - \mathbf{k}_q \cdot \mathbf{r}_j) \sum_{l_1=0}^{L} (2l_1+1) \left| h_{l_1}^{(2)}(k_0 r_t) \right|^2 P_{l_1}\left(\hat{k}_p \cdot \hat{k}_q\right).$$

Here, Equation (15) has used the symmetry of $\hat{k}_p$ and $\hat{k}_q$ about spherical center. When $K = \max\{K_1, K_2\} \to \infty$:

$$A_{i,j} = \lim_{K\to\infty} \bar{A}_{i,j} \ , \ B_{i,j} = \lim_{K\to\infty} \bar{B}_{i,j}. \tag{16}$$

Obviously, $A_{i,j}$ and $B_{i,j}$ are proved to be pure real when the test points approximate infinite on testing spherical surface. This is the property of Green's function integral and is also the supplementary interpretation of real coefficient scheme in [7]. In practical application, we can use $\bar{A}_{i,j}$ and $\bar{B}_{i,j}$ to approximate $A_{i,j}$ and $B_{i,j}$, and the fitting coefficients are real values, which can make computation efficiency improved greatly.

2.3. RFGG-FG-FFT for CFIE

For translating the complex value expression of fitting coefficients in FGG-FG-FFT into the real expression, new fitting technique is proposed as:

1). According to fitting matrix Equation (8), substitute $A_{i,j}$ and B_i^p by their approximation $\bar{A}_{i,j}$ and $\bar{B}_{i,j}$ which are decided by truncated Green's function having the number of modes $L = kd + 5\ln(\pi + kd)$, in which $d = \sqrt{3}Mh$. $\bar{A}_{i,j}$ and $\bar{B}_{i,j}$ have the expression similar to Eq. (15).

2). Solve Eq. (8) to achieve pure real fitting coefficients.

Define $\mathrm{RE}(g)$ and $\mathrm{RE}(\nabla g)_\sigma$ as:

$$\begin{aligned} \mathrm{RE}(g) &= \frac{\left| g(\mathbf{r}, \mathbf{r}') - \sum_{u=1}^{(M+1)^3} \pi_{u,Cm}^{\mathbf{r}} g(\mathbf{r}_u, \mathbf{r}') \right|}{|g(\mathbf{r}, \mathbf{r}')|}, \\ \mathrm{RE}(\nabla g)_\sigma &= \frac{\left| (\nabla g(\mathbf{r}, \mathbf{r}'))_\sigma - \sum_{u=1}^{(M+1)^3} (\varsigma_{u,Cm}^{\mathbf{r}})_\sigma g(\mathbf{r}_u, \mathbf{r}') \right|}{|(\nabla g(\mathbf{r}, \mathbf{r}'))_\sigma|}, \end{aligned} \tag{17}$$

which reflect the relative errors of fitting Green's function and the gradient of Green's function, respectively. It is noticeable that in Eq. (8) with the truncated Green's function $[A]^+$ and $[B^p]$ have some common terms during the whole fitting process for all of the fitted points. $[A]^+$ can be used repeatedly because it only concerns common grid cube. However for different fitted points, $[B^p]$ needs to be computed respectively except for the common terms. As a consequence, the complexity during computing fitting coefficients does not increase so greatly that consuming time during this process can be neglected.

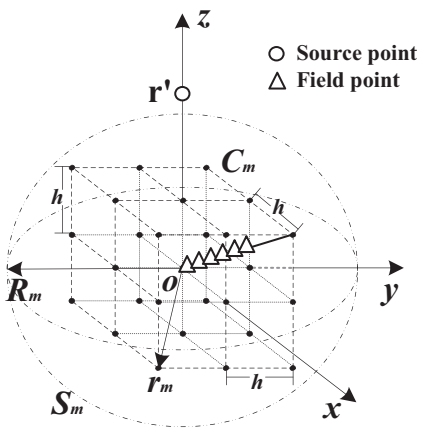

Figure 1. Fitted field point in grid cube with $M = 2$, source point $\mathbf{r}' = (0, 0, 0.3\lambda)$.

Figure 1 shows a case for evaluating new fitting technique. It gives a set of Cartesian grid nodes with expansion order $M = 2$ enclosing fitted field point, a fixed source point is located on z-coordinate outside this cube, whose distance to the center is not smaller than near zone boundary $d_{near} = (M+1)h$. Testing points are chosen on the spherical surface S. Rule of choosing grid cube for fitted field point is that the nearest node to fitted field point in distance is the cube's center, so the largest distance in each coordinate (x, y, z) between fitted field and cube's center is not more than $0.5h$. Let fitted field point move along this cube's diagonal line ($x = y = z$) from its center to point of ($0.5h$, $0.5h$, $0.5h$).

Set $h = 0.1\lambda$ (λ is wavelength in the free space), fixed point $\mathbf{r}' = (0, 0, 0.3\lambda)$, $r_t = 0.3\lambda$ and $L = 11$. Green's function and three components ($\sigma = x, y, z$) of its gradient are given in Figs. 2(a)–2(d) respectively. Because fitted field point moves along the diagonal line from (0, 0, 0) to ($0.5h$, $0.5h$, $0.5h$), its coordinate value is expressed as $x = y = z$ ($0 \le x \le 0.5h$). In Figs. 2(a)–2(d), horizontal coordinate x ranges from 0 to 0.05λ. Subscripts 1, 2 stand for new fitting technique, original technique in FGG-FG-FFT respectively. FGG-FG-FFT still utilizes the original technique in Eq. (7). Generally, when the testing points reach more than 10 times the fitting cube's nodes, in FGG-FG-FFT fitting error keeps stable even though grid spacing is different. So set the number of testing points $T_e = 338$. Results show that when grid spacing is small, real fitting coefficients by the new fitting technique have almost the same relative error as complex fitting coefficient by original technique.

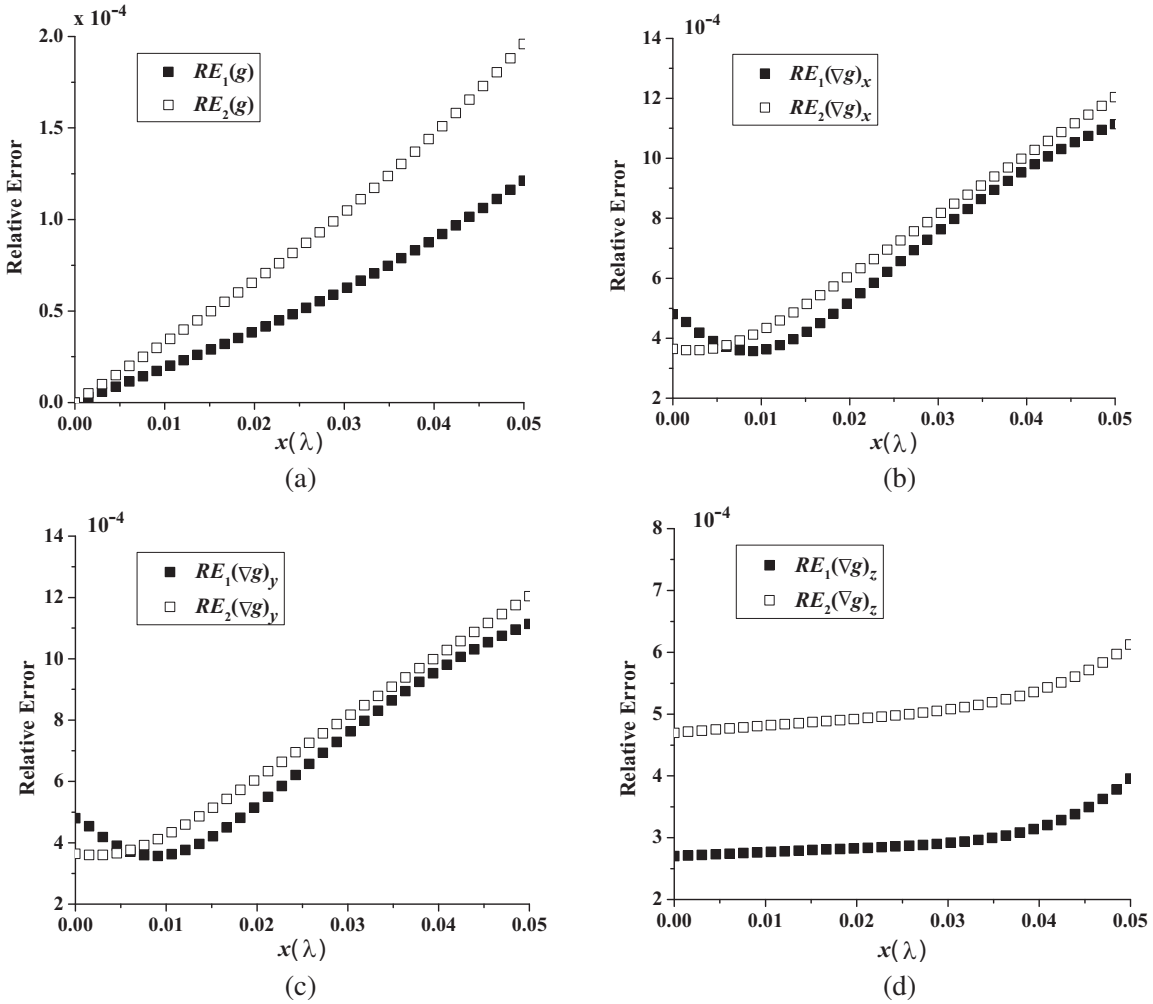

Figure 2. Relative error curves with $h = 0.1\lambda$, $\mathbf{r}' = (0, 0, 0.3\lambda)$, (a) Green's function, (b) x-component of the Green's function's gradient, (c) y-component of the Green's function's gradient, (d) z-component of the Green's function's gradient.

This example gives the comparison of relative error under special condition that source point is located right on z axis. If source points are located at any position outside of fitting cube, new fitting technique still has high accuracy comparable to original technique. The source point distance gets larger, and fitting error gets smaller.

3. NUMERICAL RESULTS AND DISCUSSION

Combine FGG-FG-FFT with new fitting technique to formulate RFGG-FG-FFT which is similar to FGG-FG-FFT except for fitting technique. Set grid spacing $h = 0.1\lambda$ or 0.2λ, expansion order $M = 2$, and near zone boundary $d_{near} = (M + 1)h$. The iteration solver BiCGSTAB is adopted, and highly efficient FFTW [13] library of OpenMP version is employed for parallel computing FFTs in per iteration. The computing platform is AMD processor of 2.3 GHz with 64 kernels and 64 GB RAM.

3.1. A PEC Sphere

For comparing RFGG-FG-FFT to FGG-FG-FFT and IE-FFT [14], a PEC sphere with radius of 6λ is illuminated by plane wave. Here is employing RWG basis functions [9] for discretizing surface with 123235 unknowns. In IE-FFT, $(M + 1) = 3$ order interpolation is adopted for Green function and its gradient. Fig. 3 shows bistatic RCS curves with different grid spacing by the above three schemes.

For comparing accuracy of three schemes, the root of mean square error (RMSE) [6] is defined for

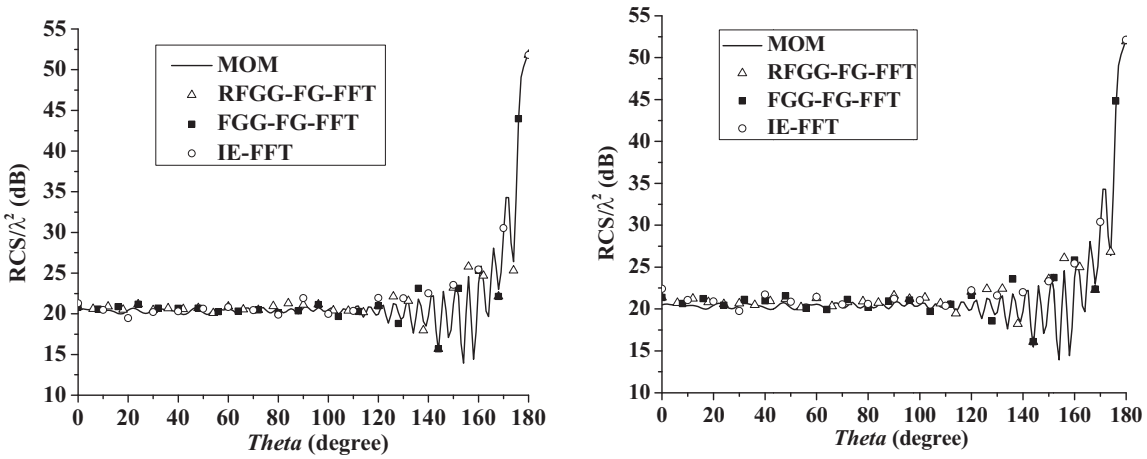

Figure 3. Comparison of three schemes with (a) $h = 0.1\lambda$ and (b) $h = 0.2\lambda$.

Table 1. Comparison of three schemes.

$h(\lambda)$		Memory of sparse coefficients (MB)	Total time (s)	*RMSE*
0.1	RFGG-FG-FFT	251.88	1182	0.10
	FGG-FG-FFT	510.47	1626	0.10
	IE-FFT	251.86	1125	0.56
0.2	RFGG-FG-FFT	240.58	887	0.12
	FGG-FG-FFT	490.84	1254	0.12
	IE-FFT	240.58	854	1.15

comparison (N is the number of unknowns of the recorded zenith).

$$RMSE = \sqrt{\frac{1}{N}\sum_{m=1}^{N}\left|(RCS/\lambda^2)^{Calculated} - (RCS/\lambda^2)^{MOM}\right|^2}. \quad (18)$$

The results with three schemes are listed in Table 1. It is obvious that: (i) RFGG-FG-FFT and FGG-FG-FFT almost have the same accuracy and are not sensitive to grid spacing, (ii) RFGG-FG-FFT has the same storage requirement as IE-FFT due to real expression for fitting coefficients, (iii) new scheme has comparable efficiency to IE-FFT, and improves computation efficiency by almost 50% compared to FGG-FG-FFT.

3.2. A PEC Brick

Figure 4 shows a PEC brick with the size of $10\lambda \times 3\lambda \times 0.2\lambda$. There are 11520 RWG functions on discretizing surface. Comparisons of bistatic RCSs from RFGG-FG-FFT, FGG-FG-FFT and p-FFT

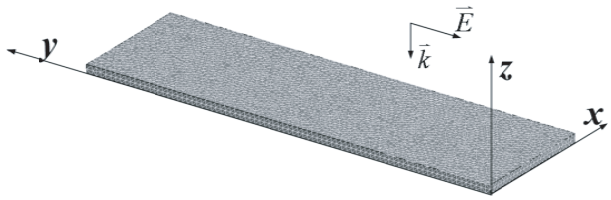

Figure 4. A PEC brick with the size of $10\lambda \times 3\lambda \times 0.2\lambda$.

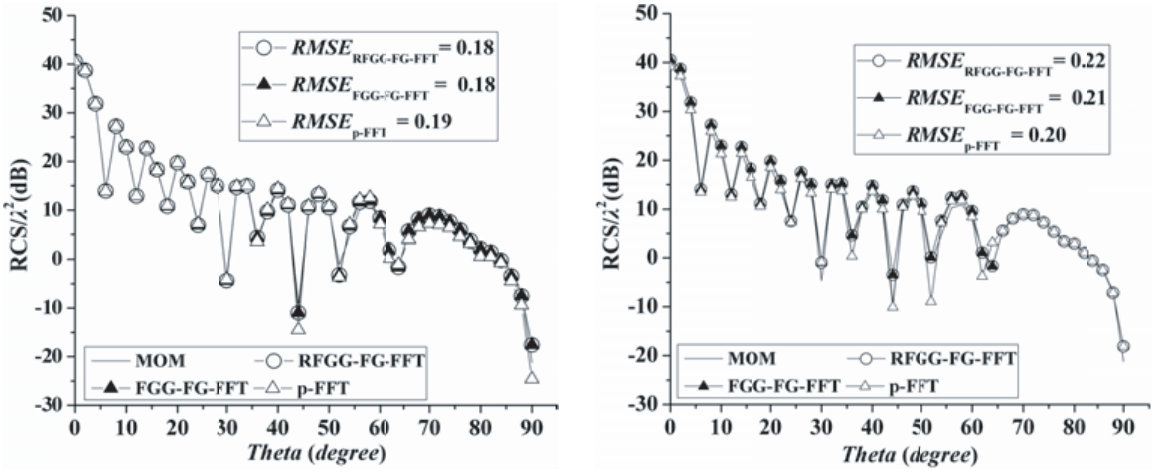

(a) (b)

Figure 5. The bistatic RCS curves of a PEC brick in yoz plane with $M = 2$, (a) $h = 0.1\lambda$, (b) $h = 0.2\lambda$.

Table 2. Comparison of three schemes.

$h(\lambda)$		Memory of sparse coefficients (MB)	Total time (s)
0.1	RFGG-FG-FFT	24.34	108
	FGG-FG-FFT	50.68	189
	p-FFT	50.21	195
0.2	RFGG-FG-FFT	24.78	85
	FGG-FG-FFT	48.34	165
	p-FFT	47.25	159

are illustrated in Fig. 5. Incident wave travels forward in $-z$ direction. The bistatic RCS curves are calculated with grid spacing $h = 0.1\lambda$, 0.2λ shown in Figs. 5(a), 5(b) respectively. RMSE of three schemes is compared to that of MOM. Results indicate that RFGG-FG-FFT and FGG-FG-FFT keep the same, stable accuracy with different h, and is in good agreement with p-FFT. Simultaneously, Table 2 indicates that RFGG-FG-FFT is more efficient than FGG-FG-FFT and p-FFT, for which RFGG-FG-FFT adopts real value expression of fitting coefficients, whereas FGG-FG-FFT and p-FFT adopt complex value expression for fitting coefficients and projections of basis function respectively. So RFGG-FG-FFT is correct and effective.

4. CONCLUSION

This paper gives an equivalent form of fitting matrix equation based on Moore-Penrose generalized inverse. Furthermore, the property of Green's function integral is proved by addition theorem. Then a new fitting technique is proposed. Numerical analysis of error shows that this new fitting technique keeps high accuracy compared to original technique in FGG-FG-FFT. Eventually a new scheme of RFGG-FG-FFT for CFIE to compute electromagnetic scattering is presented by combining FGG-FG-FFT with new fitting technique. Numerical examples show that this scheme keeps high accuracy compared to FGG-FG-FFT and p-FFT, realizes reduction of sparse matrices storage in FGG-FG-FFT, reaches 50% close to storage requirement in IE-FFT, and improves computation efficiency by almost 50% compared to FGG-FG-FFT. Like original FGG-FG-FFT, new scheme is not sensitive to grid spacing, so under the condition of larger grid spacing, the new scheme can improve computation efficiency further.

ACKNOWLEDGMENT

This work was supported by the National Natural Science Foundation of China (grant 61372033).

REFERENCES

1. Harrington, R. F., *Field Computation by Moment Methods*, Oxford University Press Oxford, England, 1996.
2. Bleszynski, M., E. Bleszynski, and T. Jaroszewicz, "AIM: Adaptive integral method for solving large-scale electromagnetic scattering and radiation problems," *Radio Sci.*, Vol. 31, No. 5, 1225–1251, Sep.–Oct. 1996.
3. Nie, X.-C., J. L.-W. Li, and N. Yuan, "Precorrected-FFT algorithm for solving combined field integral equations in electromagnetic scattering," *Journal of Electromagnetic Waves and Applications*, Vol. 16, No. 8, 574–577, 2002.
4. Yang, K. and A. E. Yilmaz, "Comparison of pre-corrected FFT/adaptive integral method matching schemes," *Microw. and Opt. Tech. Lett.*, Vol. 53, No. 6, 1368–1372, Jun. 2011.
5. Mo, S. S. and J.-F. Lee, "A fast IE-FFT algorithm for solving PEC scattering problems," *IEEE Trans. Magn.*, Vol. 41, No. 5, 1476–1479, May 2005.
6. Xie, J. Y., H. X. Zhou, W. Hong, W. D. Li, and G. Hua, "A highly accurate FGG-FG-FFT for the combined field integral equation," *IEEE Trans. Antennas Propag.*, Vol. 61, No. 9, 4641–4652, Sep. 2013.
7. Xie, J. Y., H. X. Zhou, X. Mu, G. Hua, W. D. Li, and W. Hong, "p-FFT and FG-FFT with real coefficients algorithm for the EFIE," *J. Southeast Univ.*, Vol. 30, No. 3, 267–270, Sep. 2014.
8. Abramowitz, M. and I. A. Stegun, *Handbook of Mathematical Functions*, Dover, New York, 1965.
9. Rao, S. M., D. Wilton, and A. W. Glisson, "Electromagnetic scattering by surfaces of arbitrary shape," *IEEE Trans. Antennas Propag.*, Vol. 30, 409–418, May 1982.
10. McLaren, A. D., "Optimal numerical integration on a sphere," *Math. Comp.*, Vol. 17, No. 84, 361–383, Oct. 1963.

11. Song, J., C. C. Lu, and W. C. Chew, "Multilevel fast multipole algorithm for electromagnetic scattering by large complex objects," *IEEE Trans. Antennas Propag.*, Vol. 45, No. 10, 1488–1493, Oct. 1997.
12. Stratton, J. A., *Electromagnetic Theory*, McGraw-Hill Book Company, New York, 1941.
13. Frigo, M. and S. Johnson, *FFTW Manual*, [Online]. Available: http://www.fftw.org/.
14. Xie, J. Y., H. X. Zhou, W. D. Li, and W. Hong, "IE-FFT for the combined field integral equation applied to electrically large objects," *Microw. and Opt. Tech. Lett.*, Vol. 54, No. 4, 891–896, Apr. 2012.